Cell-autonomous timing drives the vertebrate segmentation clock's wave pattern

Laurel A. Rohde[1,2,†], Arianne Bercowsky-Rama[1,5,†], Guillaume Valentin[3], Sundar Ram Naganathan[1,4,6], Ravi A. Desai[2,7], Petr Strnad[1,8], Daniele Soroldoni[1,2,9], and Andrew C. Oates[1,2,4,*]

[1]Institute of Bioengineering, Swiss Federal Institute of Technology in Lausanne EPFL; Lausanne, CH

[2]Department of Cell and Developmental Biology, University College London; London, UK

[3]Center of PhenoGenomics, Swiss Federal Institute of Technology in Lausanne EPFL; Lausanne, CH

[4]The Francis Crick Institute; London, UK

[5]Current address: bercowskya@gmail.com

[6]Current address: Department of Biological Sciences, Tata Institute of Fundamental Research; Mumbai, India

[7]Current address: University of Oxford; Oxford, UK

[8]Current address: Viventis Microscopy Sárl; Lausanne, CH

[9]Current address: Vienna BioCenter Core Facilities GmbH; Vienna, AU

†Equal contribution

*Corresponding author. Email: andrew.oates@epfl.ch

Abstract

Rhythmic and sequential segmentation of the growing vertebrate body relies on the segmentation clock, a multi-cellular oscillating genetic network. The clock is visible as tissue-level kinematic waves of gene expression that travel through the pre-somitic mesoderm (PSM) and arrest at the position of each forming segment. Here we test how this hallmark wave pattern is driven by culturing single maturing PSM cells. We compare their cell-autonomous oscillatory and arrest dynamics to those we observe in the embryo at cellular resolution, finding similarity in the relative slowing of oscillations and arrest in concert with differentiation. This shows that cell-extrinsic signals are not required by the cells to instruct the developmental program underlying the wave

pattern. We show that a cell-autonomous timing activity initiates during cell exit from the tailbud, then runs down in the anterior-ward cell flow in the PSM, thereby using elapsed time to provide positional information to the clock. Exogenous FGF lengthens the duration of the cell-intrinsic timer, indicating extrinsic factors in the embryo may regulate the segmentation clock via the timer. In sum, our work suggests that a noisy cell-autonomous, intrinsic timer drives the slowing and arrest of oscillations underlying the wave pattern, while extrinsic factors in the embryo tune this timer's duration and precision. This is a new insight into the balance of cell-intrinsic and -extrinsic mechanisms driving tissue patterning in development.

Introduction

As the vertebrate embryo develops, a multi-cellular patterning system called the segmentation clock translates the rhythm of genetic oscillations into the successive and periodic formation of tissue segments (A. C. Oates, Morelli, and Ares 2012). These segments, called somites, give rise to the metameric backbone, ribs and associated muscles of the adult body. The segmentation clock's dynamics are visible in the embryo as tissue-level waves of gene expression that travel anteriorly through the presomitic mesoderm (PSM) until they arrest at the position of the newly forming somite (Alexander Aulehla et al. 2008; Delaune et al. 2012; Masamizu et al. 2006; I Palmeirim et al. 1997; Soroldoni et al. 2014). Waves are produced by the slowing of oscillations in cells as they mature and flow anteriorly through the spatial reference frame of the PSM; this slowing creates a phase shift along the anteroposterior axis (Delaune et al. 2012; Morelli et al. 2009; Shih et al. 2015; Yoshioka-Kobayashi et al. 2020). Here we investigate what drives the cellular-level slowing of oscillations and clock arrest; in particular, we wish to determine the balance of cell-intrinsic and -extrinsic factors in this patterning process.

Previous work has implicated both cell-intrinsic mechanisms and extrinsic signals in driving the slowing of oscillations and clock arrest. These mechanisms include morphogen signaling gradients across the PSM (Ishimatsu et al. 2010, Diaz 2020, Moreno and Kintner, 2004; Sawada et al., 2001; Simsek and Özbudak, 2018), the decay of signaling factors carried anteriorly by PSM cells (Aulehla et al., 2003; Dubrulle and Pourquié, 2004), the counting of oscillations (I Palmeirim et al. 1997; Zákány et al. 2001), the comparison of oscillators' phases within cells (Sonnen et al. 2018), and neighboring cells comparing their oscillations (Boareto, Tomka, and Iber 2021; Murray, Maini, and Baker 2011). However, definitive evidence with respect to the slowing and stopping of oscillations in the embryo is lacking due to the experimental challenges of deconstructing the segmentation clock. The relative balance of cell-intrinsic versus -extrinsic information therefore remains an open question.

The classical test for intrinsic properties is to isolate cells from their neighbors and the tissue environment, then observe their autonomous behavior in culture. Cell culture systems derived from explanted primary material and induced stem cells have been developed with the aim to recapitulate clock dynamics and segmentation (Diaz Cuadros and Pourquie 2021; Pourquié 2022). Isolated PSM cells have been shown to autonomously oscillate in various permissive culture conditions (Andrew C Oates 2020). Isolated human and mouse PSM cells derived from stem cells showed autonomous, sustained oscillations upon inhibition of YAP signaling (Diaz-Cuadros et al. 2020; Matsuda, Hayashi, et al. 2020). Similarly, primary PSM cells from mouse showed sustained oscillations upon either YAP signaling inhibition (Hubaud et al. 2017; Yoshioka-Kobayashi et al. 2020) or use of a BSA-coated substrate (Hubaud et al. 2017), and zebrafish primary PSM cells

exhibited sustained noisy oscillations upon addition of FGF8 (Webb et al. 2016). In none of these cases, however, was an oscillatory pattern observed for isolated cells that resembled the slowing frequency profile expected to underlie the *in vivo* wave pattern. Recently, we reported transient (non-steady-state) oscillations in zebrafish primary PSM cells cultured without signaling molecules, small molecule inhibitors, serum, or BSA (Negrete JR et al. 2021), yet it remains unclear how these oscillations relate to the wave pattern in the embryo. Here, by quantitative comparison of dynamics in culture and in the intact zebrafish embryo, we show that isolated PSM cells have a cell-autonomous, intrinsic program capable of producing the wave pattern.

Results

Cell-autonomous transient dynamics in concert with PSM differentiation

To analyze transient dynamics from cells originating within a defined anteroposterior region of the PSM, we dissected out the posterior-most quarter of the PSM (PSM4) (Figure 1A). Each PSM4 explant was separately dissociated manually in DPBS (-$CaCl_2$, -$MgCl_2$) and cultured at low-density on protein A-coated glass in L15 medium without added signaling molecules, small molecule inhibitors, serum, or BSA (N = 11 embryos). Oscillation and arrest dynamics were followed using Her1-YFP, a fluorescently-tagged core clock component, previously used to define the zebrafish clock's tissue-level wave pattern in *Tg(her1:her1-YFP)* embryos, called *Tg(her1-YFP)* here (Soroldoni et al., 2014), and a novel Mesp-ba-mKate2 transgene *Tg(mesp-ba:mesp-ba-mKate2)*, called *Tg(mesp-ba-mKate2)* here, which marks the rostral half of the forming somite in the anterior PSM (Figure 1A-C; Figure 1 – figure supplement 1), as expected (Cutty et al. 2012). Mesp2 has been used in multi-cellular segmentation clock cultures as a marker of differentiation upon clock arrest (Diaz-Cuadros et al. 2020; Lauschke et al. 2013; Matsuda, Yamanaka, et al.

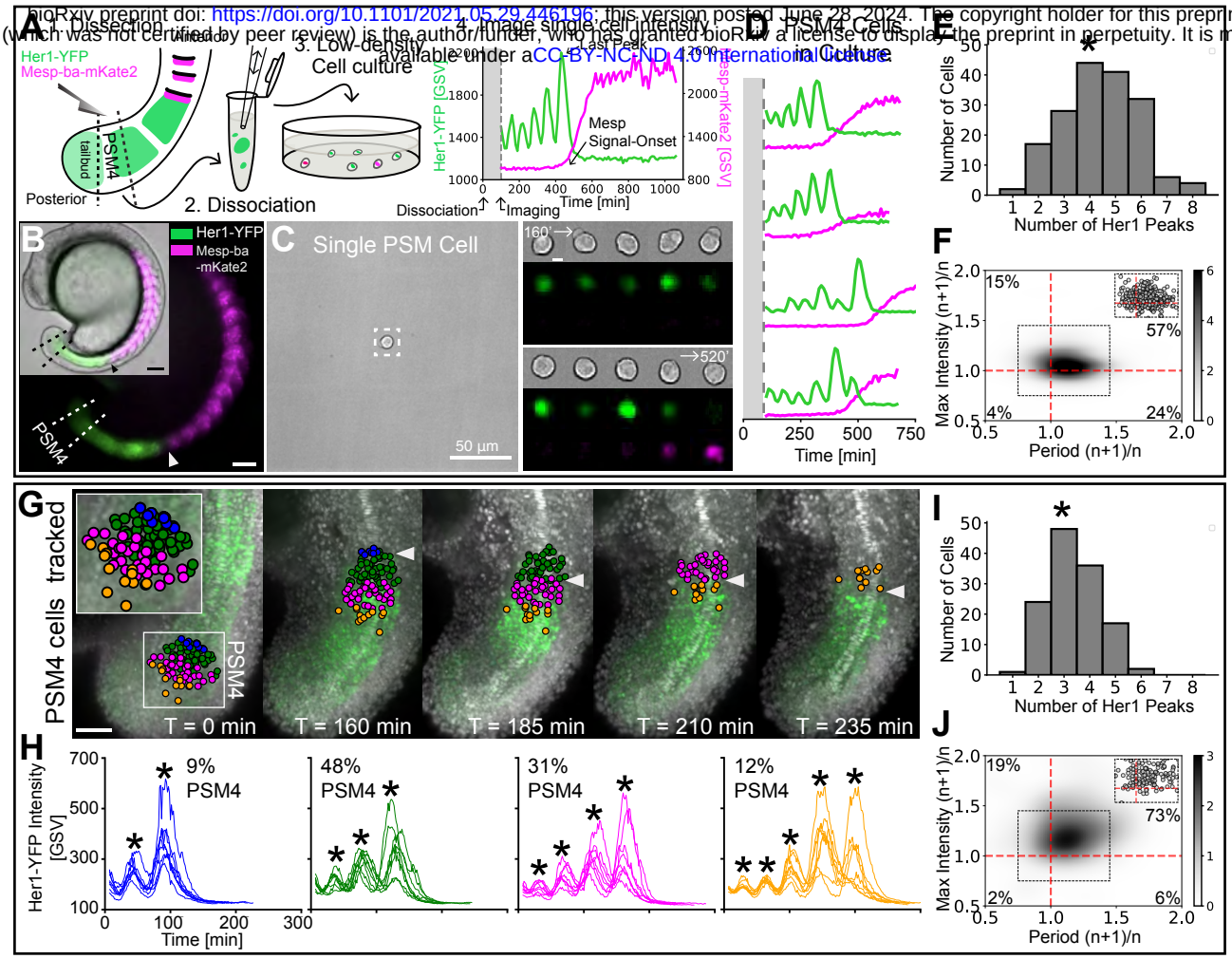

Figure 1. Cell-autonomous oscillatory dynamics reproduce those underlying wave pattern in the embryo.

(A) Experimental design: 1) Dissection of posterior-PSM quarter (PSM4) (dashed lines) from a *Tg(her1-YFP;mesp-ba-mKate2)* 15 somite-stage embryo, 2) Dissociation into single cells, 3) Culture at low-density, and 4) Her1-YFP and Mesp-ba-mKate2 imaging over time. **(B)** Her1-YFP and Mesp-ba-mKate2 in a 15 somite-stage *Tg(her1-YFP;mesp-ba-mKate2)* embryo (bright-field inset). Arrowheads mark the recently formed somite (S1). Dissection lines surround PSM4. Scale bar 100 μm. **(C)** One cell per field of view imaged. Boxed region over time (scale bar 5 μm). Intensity trace shown in A. **(D)** Representative intensity traces of PSM4 cells in culture. **(E)** Number of Her1-YFP peaks (*mean ± SD, 4.4 ± 1.6 peaks) per PSM4 cell in culture (N = 11 embryos, n = 174 cells). **(F)** Density plot of ratios of successive Her1-YFP periods and peak intensity ($cycle^{n+1}/cycle^{n}$) for PSM4 cells in culture (n = 421 successive cycle ratios, circles in inset). Percent of total ratios per quadrant is indicated. **(G,H)** PSM4 cells in a *Tg(her1-YFP;h2b-mCherry)* embryo tracked until somite formation (arrowhead) (N = 2 embryos, n = 128 PSM4 cells). Scale bar 100 μm. Cells contributing to the same somite are identically coloured in the embryo and representative Her1-YFP intensity traces (* peaks). Percentage of tracked PSM4 cells contributing to a given somite is shown. **(I)** Number of Her1-YFP peaks (*mean ± SD, 3.4 ± 1.0 peaks) per PSM4 cell in the embryo. **(J)** As described in F with PSM4 cells in the embryo (n = 179 total successive cycles).

2020; Matsumiya et al. 2018; Tsiairis and Aulehla 2016). Analysis of Her1-YFP and Mesp-ba-mKate2 intensity was carried out in single *Tg(her1-YFP;mesp-ba-mKate2)* cells that survived over 5 hours post-dissociation, remained the only cell in the field of view, did not divide, and showed transient Her1-YFP dynamics (Figure 1 – figure supplement 2).

Single PSM4 cells in culture produced Her1-YFP oscillations with 1 to 8 peaks before arresting (N = 11 embryos, n = 174 cells; Figure 1D,E). These oscillations typically slowed then abruptly arrested (Figure 1D,F; Figure 1 – figure supplement 3). Oscillation arrest, marked by the last Her1-YFP peak, was also associated with Mesp-ba-mKate2 signal-onset (Figure 1A,D**)**, suggesting that arrest occurs in concert with differentiation as expected from the tissue-level pattern. These transient dynamics were independent of cell-survival time in culture (Figure 1 – figure supplement 4), reproduced in cells isolated one-per-well (Figure 1 – figure supplement 5) and did not require *Tg(mesp-ba-mKate2)* (Figure 1 – figure supplement 6). Despite inevitable uncertainty in the exact A/P boundaries of the explanted PSM4 due to manual dissection, the overall variation in arrest timing was not due to differences between the individual embryos or experiments (Figure 1 – figure supplement 7), thus limiting its source to heterogeneity within the starting PSM4 cell population and/or to the noise in an intrinsic process. Taken together, our data show that PSM4 cells autonomously slow oscillations and arrest the clock in concert with expression of a segmental differentiation marker.

Cell-Autonomous PSM transient dynamics mirror those in the embryo

To see whether the PSM4 cell-autonomous clock dynamics in culture recapitulated those produced in the embryo, we tracked cells that originated from PSM4 then flowed anteriorly until somite

formation using light-sheet imaging of freely-growing *Tg(her1-YFP;h2b-mCherry)* embryos (Figure 1G). Retaining their initial local anteroposterior arrangement, cells from the PSM4 region predominantly contributed to two of four somites and differed by at most one Her1-YFP peak within a somite (N = 2 embryos, n = 128 cells; Figure 1G,H; Figure 1 – supplement figure 8). To normalize for a general slowing of developmental time observed in zebrafish culture, as well as the overall longer periods of PSM4 cells in culture (Langenberg, Brand, and Cooper 2003; Webb et al. 2016; Matsuda, Hayashi, et al. 2020) (Figure 1 – supplement figure 9), we used the number of peaks generated and the ratio of successive periods and peak intensities to compare cell dynamics, rather than absolute time. Cells in culture produced on average more peaks and showed increased variability in the number of peaks compared to cells in the embryo (mean ± SD = 4.4 ± 1.6 peaks in culture, COV 0.36; 3.4 ± 1.0 peaks in the embryo, COV 0.29; Figure 1E,I; Figure 1 – supplement figure 9), indicating a longer and more variable duration of the cell-autonomous transient dynamics. Because the cells tracked in the embryo originated from the same starting population as those in culture, these results suggest that the variability in culture is not due to a difference in initial heterogeneity within that cell population, but reflects an increase in the noise of the cell-autonomous dynamics.

The key dynamic of successive period slowing was shared between PSM4 cells in culture and in the embryo (81% of successive cycles slowed in culture vs 79% in the embryo; Fig 1F,J; Figure 1 – supplement figure 10C,E). However, a rise in intensity from one peak to the next was seen less often in culture (72% successive cycles in culture and 92% in the embryo; Fig 1F,J; Figure 1 – supplement figure 10B,D), and there was less of a correlation between intensity rise and slowing in the culture than in the embryo (57% of successive cycles both slow and rise in culture vs 73%

in the embryo; Fig 1F,J). These differences in accompanying intensity rise show that although the cell-autonomous program generates slowing oscillations, the amplitude of the oscillations is noisier, suggesting that this feature may be tuned by extrinsic factors in the tissue.

We next asked whether Her1-YFP arrest and Mesp-ba-mKate2 signal-onset in the culture reflected the spatiotemporal pattern of these events in a forming somite in the embryo. To systematically address this question, we backtracked all the cells in the recently formed somite (S1) in a *Tg(her1-YFP;h2b-mCherry)* embryo and *Tg(mesp-ba-mKate2;h2a-GFP)* embryo (Figure 2A,B). All cells in the somite expressed Her1-YFP and most produced a last peak in the prospective somite (S -1), creating a phase profile across the future rostral-caudal somite axis that reflected the tissue-level wave's arrival (n = 233 cells, Figure 2C,D). Thus, in the embryo, clock arrest of all the cells that form a single somite does not occur simultaneously, but is nevertheless spatiotemporally limited within S-1. Similar to the embryo, most PSM4 cells in culture that survived past 5 h and remained undivided were found to oscillate and arrest Her1-YFP (Figure 1 – supplement figure 2).

Mesp-ba-mKate2 was first detected within the forming somite (S0), with higher levels rostrally. We defined Mesp-ba-mKate2 signal-onset times in intensity traces from cells in the embryo and in culture that had a clear intensity rise (Figure 2 – supplement figure 1A). The distribution of Mesp-ba-mKate2 intensity rise and proportion of cells with a clear signal-onset time in the embryo was comparable to that seen within the PSM4 cells in culture (N = 2; Figure 2 – supplement figure 1A,B), suggesting that there is no cell-autonomous default state, i.e. Mesp "on" or "off".

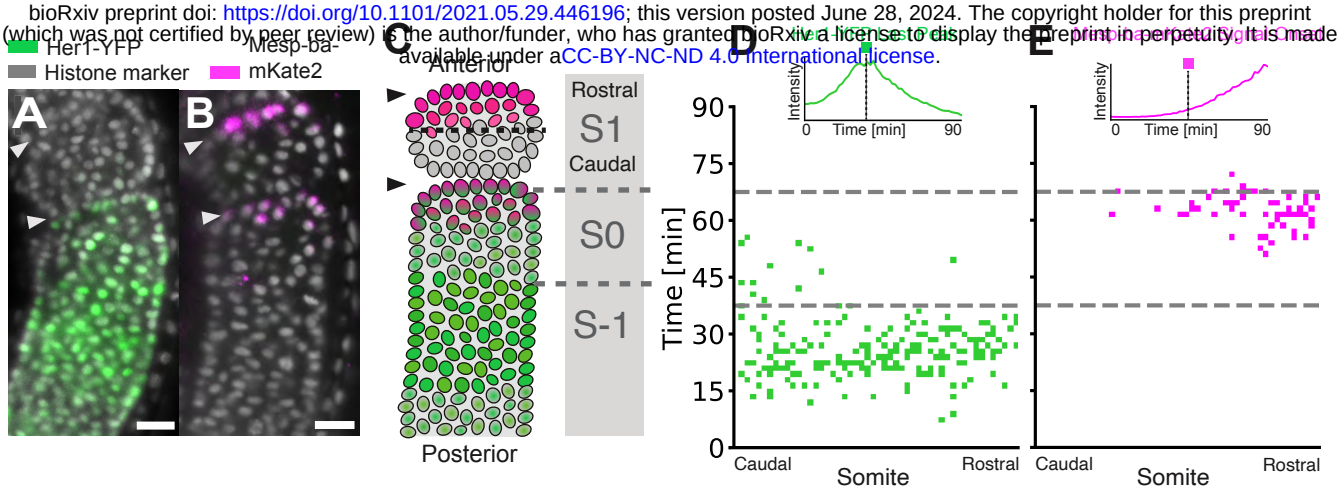

Figure 2. Clock arrest and Mesp-ba-mKate2 signal-onset within the forming somite.

(A, B) Her1-YFP in a *Tg*(*her1-YFP;h2b-mCherry)* embryo (A) and Mesp-ba-mKate2 in a *Tg(mesp-ba-mKate2a;h2a-GFP)* embryo (B). Representative lateral PSM light-sheet slice. Scale bar is 25 μm. Arrowheads at somite boundaries. **(C)** Cartoon of the formed somite (S1), the forming somite (S0) and the prospective somite (S-1). **(D, E)** S1 cells backtracked in a *Tg*(*her1-YFP;h2b-mCherry)* embryo (n = 233 cells) (D) and a *Tg(mesp-ba-mKate2a;h2a-gfp)* embryo (n = 190 cells) (E). Kymograph of Her1-YFP last peak (D) and Mesp-ba-mKate2 signal-onset time (E) in cells relative to the rostral-caudal somite axis (inset with example traces). Dashed grey line at transitions S-1 to S0 and S0 to S-1.

To directly compare the temporal relationship of Mesp-ba-mKate2 signal-onset and Her1-YFP arrest in individual cells, we backtracked from the most recently formed somite (S1) in *Tg*(*her1-YFP;mesp-mKate2*) dual-transgenic embryos. We found that Mesp-ba-mKate2 signal-onset mostly occurred after the last Her1-YFP peak in the embryo. However, this relationship was not as precise in culture, with Mesp-ba-mKate signal-onset spanning the last peak (Figure 2 – supplement figure 1C,D), indicating a loss of coordination in the transition between clock arrest and segment polarization.

The tight temporal association of clock arrest and differentiation suggests that both could rely on the same timing information across the PSM. We next asked whether this cell-autonomous timing depends on oscillations of the clock, potentially by using the accumulating cycles as a timer. To test this, we examined the timing of cell-autonomous Mesp-ba-mKate2 signal-onset in cells isolated from embryos with a genetic background lacking both *her1* and *her7* genes, a condition that disables the clock (Lleras Forero et al. 2018). We detected a similar proportion of Mesp signal-onset in control *Tg(mesp-ba-mKate2)* and *her1*$^{-/-}$; *her7*$^{-/-}$; *Tg(mesp-ba-mKate2)* cells (Figure 2 – supplement figure 2A,B), and observed comparable timing (281 ± 62 min in control cells, 305 ± 70 min in *her1*$^{-/-}$; *her7*$^{-/-}$ cells; Figure 2 – supplement figure 2C). Thus, the timing of Mesp-ba-mKate2 signal-onset appears independent of the segmentation clock's oscillations, suggesting that timing information that feeds into both the clock and differentiation across the PSM does not require oscillations.

Together, our data suggests that the slowing and arrest of oscillations underlying the wave pattern in embryos is driven cell-autonomously in differentiating PSM cells. However, the noisier dynamics of the cell-autonomous program suggest that extrinsic signals present in the embryo may

adjust the time of clock arrest in concert with differentiation, and sharpen clock oscillatory dynamics.

FGF extends the cell-autonomous clock and differentiation program in cultured posterior PSM cells.

We next explored whether FGF, an extrinsic signal known to affect segmentation, interacts with the cell-autonomous program by culturing PSM4 cells in the presence of FGF8 (Figure 3A,B; Figure 3 – supplement figure 1). A gradient of FGF signaling has been shown to extend from the tailbud across the PSM and has been postulated to provide spatiotemporal information to the segmentation clock (Dubrulle and Pourquié 2004; 2004; Sawada et al. 2001; Akiyama et al. 2014; Sari et al. 2018). Previous experiments implanting FGF8-soaked beads adjacent to posterior PSM in the embryo resulted in an extension of clock/PSM activity such that somite boundary formation was delayed, yielding shorter segments (Dubrulle, McGrew, and Pourquié 2001; Sawada et al. 2001). Consistent with this delay in the embryo, we found that addition of FGF8 to the culture medium extended the cell-autonomous program in PSM4 cells, doubling the mean number of oscillations generated per cell (Figure 3C) and shifting the Her1-YFP last peak to later times (Figure 3D). Notably, exogenous FGF did not reduce noise in the cell-autonomous program (Figure 3C,D; Figure 3 – supplement 2).

Despite the Her1-YFP last peak occurring later on average, it retained a temporal association with Mesp-ba-mKate2 signal-onset in the presence of FGF (Figure 3 – supplement figure 3A) and the distribution of Mesp-ba-mKate2 intensity traces was not altered (Figure 3 – supplement figure 3B). Interestingly, a small subset of cells (5 out of 54 cells) produced multiple Her1-YFP

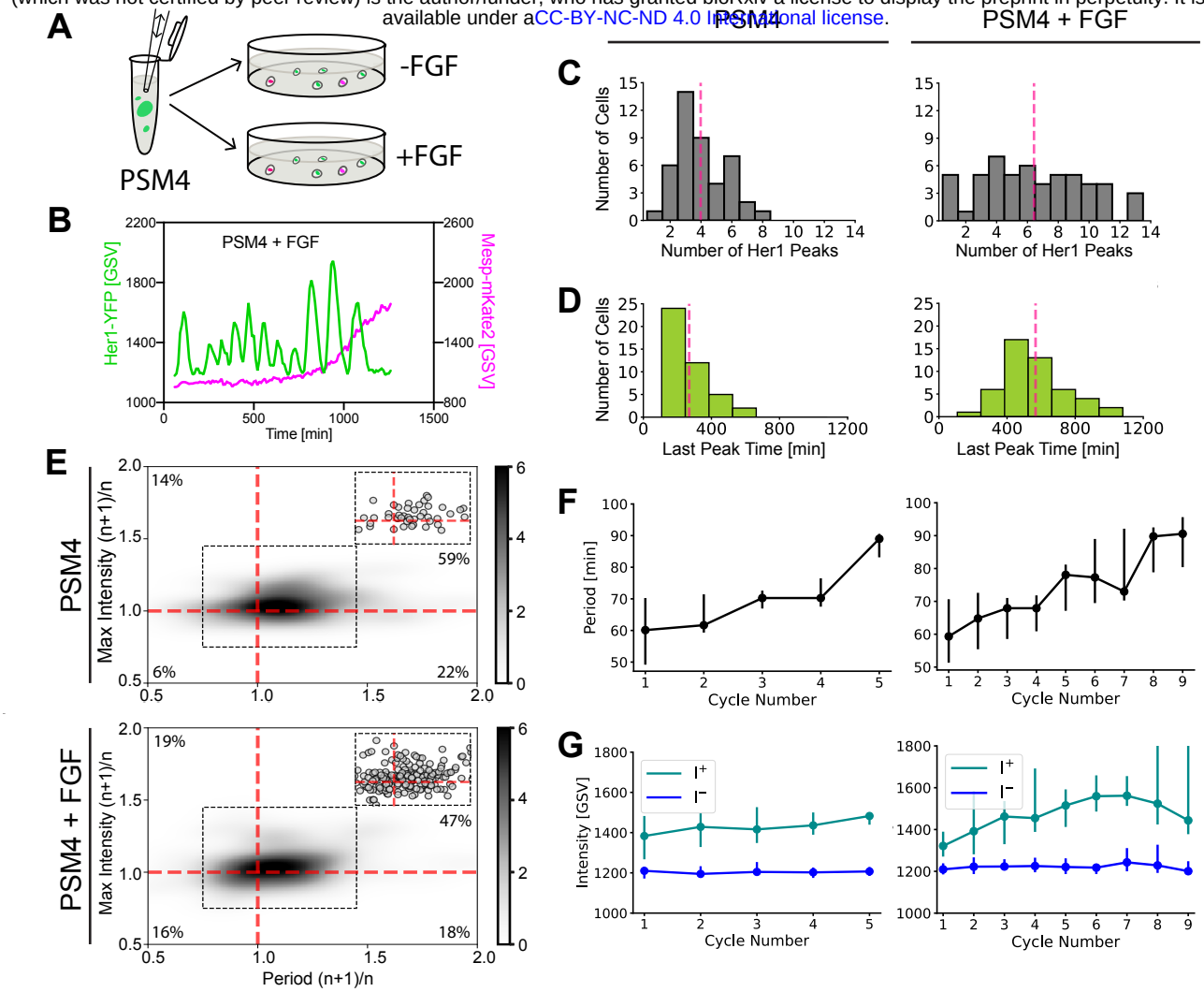

Figure 3. FGF extends cell-autonomous program duration of PSM4 cells in culture.

(A) A pool of dissociated PSM4 cells was split into a control well and one containing FGF-8b, then cultured (N = 4 experiments, n = 44 PSM4 control cells and n = 54 PSM4 cells with added FGF. **(B)** Representative Her1-YFP and Mesp-mKate2 trace from PSM4 cells cultured with added FGF. **(C)** Number of Her1-YFP Peaks produced per cell, with pink line at the mean (mean ± SD = 4.0 ± 1.8 peaks in control cells, 6.4 ± 3.5 with FGF). **(D)** Time of Her1-YFP last peak (min post-dissociation), with pink line at the mean (mean ± SD = 269 ± 116 min post-dissociation in control cells, 568 ± 185 min post dissociation in cells with FGF. **(E)** Ratio of successive cycle Her1-YFP periods (Period (n +1)/n) and peak intensity (Max Intensity (n+1)/n). Upper right quadrant indicates successive intensity rise and oscillation slowing. n = 51 successive cycle ratios in PSM4 control cells and n = 196 in PSM4 cells cultured with FGF, shown as circles in inset and percent of successive cycles is indicated in each quadrant. **(F,G)** All Her1-YFP intensity traces were aligned by the first peak. The period (F) and intensity of peaks (I+) and troughs (I-) (G) is given for each cycle as a median (circle) with 25th and 75th interquartiles (bar).

oscillations after the Mesp-ba-mKate2 signal-onset (Figure 3 – supplement figure 1), suggesting that these events can be uncoupled. Together, these results indicate that the PSM4 can cell-autonomously extend the timing of clock arrest and segmental differentiation in response to FGF.

We found that successive oscillations continued to slow overall in the presence of FGF, although in fewer successive cycles (65% in FGF-treated cells vs 81% in control; Figure 3E,F), suggesting some disorganization of the dynamics in the FGF-extended cell-autonomous program. Successive increase in peak intensity was also observed (66% of FGF-treated cells vs 73% of control; Figure 3E,G), mostly in conjunction with slowing oscillations (Figure 3E). Despite this increased noise in the cell-autonomous program, we did not observe a systematic alteration of the period and intensity in response to FGF (Figure F,G).

Together, our data shows that FGF extends the duration of the cell-autonomous program transient dynamics in a manner that could explain reported effects of FGF activity on segment boundary position in the embryo (Dubrulle, McGrew, and Pourquié 2001; Sawada et al. 2001) and supports a hypothesis that extrinsic signals act upon the clock through the cell-autonomous program.

Cell-autonomous, intrinsic timer initiates as cells exit the tailbud

We hypothesize that the cell-autonomous program of slowing oscillations and arrest in concert with differentiation is controlled by a timer that, in the embryo, encodes positional information as cells flow anteriorly. If an intrinsic timer provides positional information to the clock in the embryo, we predicted that cells located more anteriorly in the PSM will have less time remaining before arrest and differentiation. To test this, we followed oscillation and arrest dynamics in single

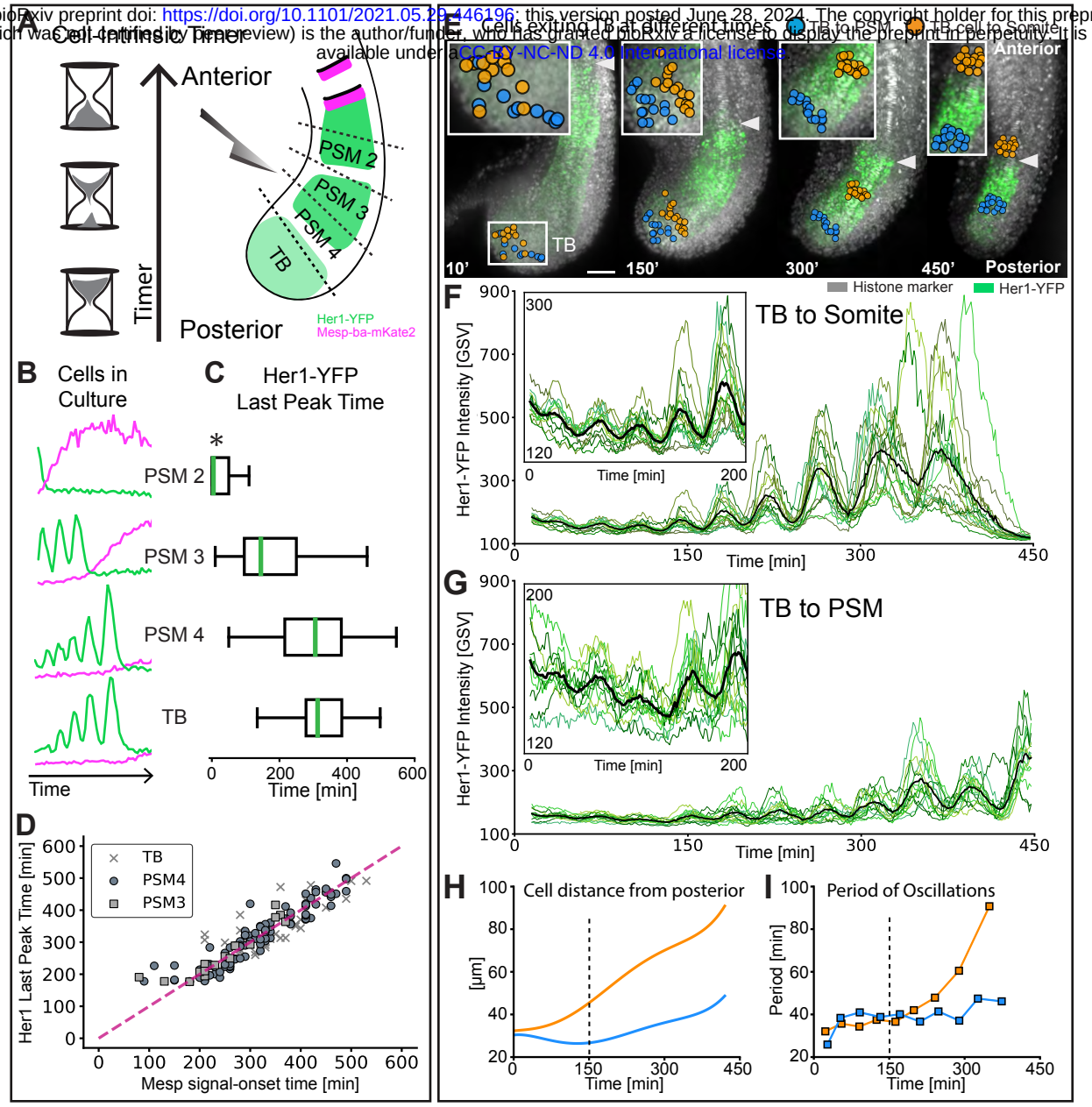

Figure 4. Intrinsic timer initiates upon TB exit and duration shortens in cell flow.

(A) Experimental design: *Tg(her1-YFP;mesp-ba-mKate2)* PSM was dissected into different anteroposterior quarters, dissociated, and then cultured. PSM4 was dissected and cultured in parallel from each embryo to serve as an internal reference. **(B)** Representative intensity traces for the different anteroposterior quarters. **(C)** Her1-YFP last peak times as median (green line) with interquartile box and whiskers. Time given as post-dissociation. Data pooled by cell type (N = 3 embryos, n = 32 PSM2 and 32 PSM4 cells; N = 3 embryos, n = 65 PSM3 and 41 PSM4 cells; N = 3 embryos, n = 38 TB and 59 PSM4 cells). PSM2 last peaks that occurred prior to the start of imaging were set to acquisition start time (*). **(D)** Correlation of Her1-YFP Last Peak and Mesp-ba-mKate2 signal-onset time. **(E)** Cells backtracked from posterior PSM (blue, n = 17) and S1 (orange, n = 15) to the TB at 15 somite stage in a representative embryo (7.5 h imaging, *Tg(her1-YFP;h2b-mCherry,* N = 2). Arrowhead at recently formed somite boundary. Scale bar 100 μm. **(F, G)** Her1-YFP intensity traces for individual cells (green) and mean intensity (black). Inset zoom of oscillations in the TB. **(H)** Cell distance from posterior tail tip. **(I)** Mean Her1-YFP period.

isolated cells originating from different anteroposterior quarters of PSM tissue in the embryo, and used PSM4 dissected from the same embryos as an internal reference (Figure 4A; Figure 4 – supplement 1A). Consistent with a timer running down in the embryo, isolated PSM cells originating more anteriorly successively slowed oscillations, but tended to produced fewer peaks than PSM4 cells and arrested Her1-YFP earlier in concert with Mesp-ba-mKate2 signal-onset (Figure 4B-D; Figure 4 -supplement figure 1A-E; Figure 4 – supplement figures 2 and 3).

To explore when this timer starts, we cultured cells from the tailbud (TB), which we define as the region posterior to the end of the notochord (Figure 4A), where Her1-YFP oscillations are present (Soroldoni et al. 2014) and progenitor cells are thought to be maintained (Martin 2016). However, unlike amniotes, zebrafish do not possess an NMP population in the tailbud that contributes substantially to the tail (Attardi et al. 2018). As we did with the PSM, we analyzed cells that survived over 5 hours post-dissociation, remained the only cell in the field of view, did not divide, and showed transient Her1-YFP dynamics. We found that single TB cells in culture oscillated with successive slowing, then arrested concurrent with Mesp-ba-mKate2 signal-onset (Figure 4B-D; Figure 4 - supplement figure 1C-E; Figure 4 – supplement 4). Moreover, TB and PSM4 dissected from the same embryos were found to arrest oscillations with similar timing, despite the more posterior origin of the TB cells (Figure 4C; Figure 4 - supplement figure 1A, B). These results suggest that experimental removal from the TB starts the intrinsic timer such that its duration is equivalent to that of cells which have recently entered the PSM. We thus propose that TB cells have already expressed the cell-autonomous timing mechanism, but require a trigger associated with exit from the TB to start the timing activity.

If the timer starts upon TB exit, then we expected that cells in the embryo initiate slowing oscillations and amplitude rise when they transition into the PSM. Cells within the TB are known to mix and remain for a range of times before joining the PSM (Mara et al. 2007). To compare the start of slowing oscillations in TB cells that join the PSM at different times, we backtracked individual cells located either within PSM4 or the most recently formed somite at the end of a 450 min time-lapse movie (Figure 4E). We observed that while in the TB, individual cells from both groups showed low-intensity, noisy Her1-YFP oscillations (Figure 4F,G), confirming that TB cells that will later become PSM in the zebrafish do oscillate. As the embryo developed, the group of cells backtracked from the recently formed somite were the first to join the PSM, at which time their oscillations slowed successively and increased in peak intensity (Figure 4H,I). These dynamics continued as cells flowed anteriorly then arrested during somite formation (Figure 4F,H,I). In contrast, the group of cells backtracked from PSM4 exited the TB later and showed a corresponding delay in slowing, and intensity rise (Figure 4G-I). This tight correlation of the initiation of slowing oscillations in cells with their exit from the TB in the embryo supports the idea that exit from the TB starts the intrinsic timer.

Discussion

The population-level behavior of the oscillators of the segmentation clock is the hallmark wave pattern. The role of short-range cell-cell signaling through the Delta-Notch pathway in the local synchronization of the oscillators is well established (Venzin and Oates 2020), providing local coherence to the wave pattern. However, the mechanism for the gradual slowing and stopping of the oscillators that creates the phase off-set required for waves at the tissue-level remains a topic

of debate. Our results clearly implicate a cell-autonomous program of slowing and stopping as the basis for the tissue-level wave-pattern in the zebrafish, and show that a universal picture of the vertebrate segmentation clock that is centered on persistent cellular oscillators instructed by extrinsic signals is inadequate. Rather, our work highlights the importance of transient dynamics driven by a cell-autonomous timing mechanism.

How the balance of cell-intrinsic dynamics and extrinsic signaling plays out in other segmentation clock systems remains to be tested. However, the concept of a cell-intrinsic timer explains the long-known intrinsic properties of explanted PSM tissue from several species to segment with periodicity and AP directionality (Alexander Aulehla and Pourquié 2006; Dubrulle, McGrew, and Pourquié 2001; Clarissa A. Henry et al. 2005; Lauschke et al. 2013; Maroto et al. 2005; I Palmeirim et al. 1997; Isabel Palmeirim et al. 1998). Indeed, the long-standing "Clock and Wavefront" model of the segmentation clock originally postulated an intracellular timing gradient as the mechanism behind the wavefront of cellular change interacting with the clock to determine somite position (Cooke and Zeeman 1976). Here we have shown that both the clock and the wavefront, comprising just such an intracellular timing mechanism, are captured in a single cell running an autonomous program.

For simplicity, we have argued for a single timing mechanism. Curiously, we observed that in cells treated by FGF, the timing of arrest of oscillations and the onset of differentiation were dissociated in approximately 10% of cells. One interpretation of this result is that there are two (or more) parallel timing mechanisms underlying the normal tight linkage of clock arrest and differentiation, and elevated FGF signaling can cause these mechanisms to uncouple in a small set of cells.

Another interpretation is that the clock arrest and onset of differentiation use different sensors of the same timer. Although these sensors react closely in time under normal circumstances, with a change in the timer's dynamics caused by FGF (for example, a lower slope of a timing gradient) the sensors react at different times in a small set of cells. Current evidence does not allow us to choose between these interpretations. A similar dissociation of clock arrest and differentiation timing has previously been inferred in the *doppelkorn* medaka mutant from gene expression patterns (Elmasri et al. 2004), suggesting the *doppelkorn* gene, when identified, may shed further light on the phenomenon.

The difference in duration and precision between cellular dynamics in the embryo and those in culture conditions distinguishes important roles of extrinsic signaling in the zebrafish segmentation clock. These roles are to regulate the length of the autonomous program and to increase the precision of the exit time in the population, so that all cells contributing to a single somite in the embryo stop oscillating within the period of somite formation. The ability of FGF to extend the duration of the program of cultured posterior PSM cells fits well with data from experiments in the embryo demonstrating that an increase or decrease in FGF activity can alter segment length (Dubruelle et al., 2001, Sawada et al., 2001). Despite the increased duration in culture, FGF did not reduce the variability of the dynamics, implying that additional signals, or temporal signaling dynamics, are important for precision at the tissue level. How the timer is triggered upon the exit of a cell from the tailbud to the PSM is likewise not known, but our experiments suggest that the rapid decrease of external signals required for maintenance of a stable oscillatory state (Hubaud and Pourquié 2014), and normally restricted to the tailbud, would explain the observed dynamics. Whether other candidate signals such as Wnt and RA (A. Aulehla and Pourquie 2010), or signal

dynamics (Sonnen et al. 2018), integrate into the control of intrinsic cell behavior to explain the timing and precision of embryonic segmentation can now be explored.

The intrinsic timer's identity and how it is tuned by extrinsic signals during development remain intriguing questions. The molecular details of the timer are not constrained by our data here, and could involve a number of plausible intermediates such as transcription factor or microRNA cascades similar to those in timing of neuroblast differentiation or *C. elegans* molting (Ambros 2011; Brody and Odenwald 2000) or phospho-timers as found in the circadian clock (Diernfellner and Brunner 2020). The latter mechanism would provide an attractive link to extrinsic signalling by FGF gradients in the PSM (Sawada et al. 2001; Simsek and Özbudak 2018). A model for slowing and then stopping oscillations via the rise and fall of Her1 production (Negrete JR et al. 2021) implies that molecules controlling *her1* transcription, such as Tbx proteins (Brend and Holley 2009) and/or Her1 translation (Dill and Amacher 2005) are involved as time-keeping factors. In this light, the activity of the Tbx-degrading factor Ripply (Wanglar et al. 2014) may play a role in the threshold at which production falls, thereby rapidly stopping the oscillations. Other models posit that the slowing of Her oscillations arise due to an increase of time-delays in the negative feedback loop of the core clock circuit (Yabe, Uriu, and Takada 2023; Ay et al. 2014), suggesting that factors influencing the duration of pre-mRNA splicing, translation, or nuclear transport may be relevant. Whatever the identity, our results suggest that the timer exerts control over differentiation independent of the clock.

Organizing animal and plant tissues and microbial assemblies with oscillatory mechanisms in naturally occurring and synthetic systems is a rapidly evolving field of interest. This includes the

investigation of the segmentation clock through innovative 3D culture models (van den Brink et al. 2020; Sanaki-Matsumiya et al. 2022). Although patterns in multicellular contexts can emerge from extrinsic signaling processes alone (Danino et al. 2010), understanding the cell-intrinsic potential within these various systems is vital to interpreting and directing population level behavior. Our work combining isolated primary cell culture and single-cell resolution imaging of the corresponding developing tissue, reveals that cell-autonomous timing directs the tissue-level patterning of the clock, and offers new opportunities to study the balance of extrinsic and intrinsic control in oscillatory patterning systems.

Methods

Zebrafish and embryo care

Wildtype (WT) and transgenic (*Tg*) fish were maintained according to standard procedures in facilities at University College London (London, UK) and Swiss Federal Institute of Technology in Lausanne EPFL (Lausanne, CH). *Tg* embryos were heterozygotes produced by natural pairwise spawning with WT (AB, TL) or another *Tg* line. The following lines have been described previously: *Tg(her1:her1-YFP)* (Soroldoni et al. 2014); *Tg(h2az2a:h2az2a-GFP)* (zfin ID: ZDB-TGCONSTRCT-070117-39) abbreviated *Tg(h2a-GFP)* here; *Tg(Xla.Eef1a1:H2Bm-Cherry)* abbreviated *Tg(h2b-mCherry)* here (Recher et al. 2013); *Def(Chr5:her1 zf2173/zf2173;her7 hu2526/hu2526)* (Lleras Forero et al. 2018). Embryos were incubated at 28.5°C in E3 without methylene blue (UCL) or facility water (EPFL) until shield stage then incubated at 19.5°C until the 8 to10 somite stage when they were screened as previously described (Soroldoni et al. 2014) and returned to 28.5°C and, prior to use, embryos were dechorionated manually in agarose-coated petri-dishes.

mesp-ba-mKate2 transgenesis

Transgenesis was performed as described previously (Soroldoni et al. 2014). In short, *mKate2* was fused to the 3' end of *mesp-ba* so as to generate a C-terminal fusion protein, then the modified BAC was subcloned to obtain a 15 kb construct. The resulting BAC was co-injected with I-Sce Meganuclease (Roche) at a concentration of 100 ng/µl and a bolus size of 130 µm. Transient expression in F0 embryos was used as a proxy to confirm the functional expression of the Mesp-ba-mKate2 fusion protein and all embryos were raised to adulthood. In total, 9 independent transgenic founders (out of 29 fish) were identified by whole-mount in situ hybridization using a probe to *mKate2*, yielding a transgenesis frequency of 30%. Based on the optimal signal to noise ratio, and the *mKate2* stripe pattern, a single founder was selected. Heterozygous and homozygous *Tg(mesp-ba:mesp-ba-mKate2)* were viable, fertile, and stably expressed mKate2 through multiple generations over 10 years.

The following primers were used for tagging and subcloning:

Forward Primer Mesp-ba tagging:

TTTACGGAAAAAACTTTGGCTATCATCTCGTTCCTCAGACTTACTGGAGAAGCTCAG GAGGTAGCGGC

Reverse Primer Mesp-ba tagging:

ACACAATACAGTATCCGCCCTCAGTTTTTGGTGTGATGGAGATCTTTCCGCGTCAGT CAGTACCGTTCG

Forward Primer shaving:

CCAAATTAGGTTAGATTAGTTACTCATCCTGGTAGCTGTACAAATAGATATAGGGAT AACAGGGTAATTGCAC

TGAAATCTAGA

Reverse Primer shaving:

CCCTGCAGTACACTGAATCTACCATGACACCATATCTTATCTTTCCAGCCccgTAGGG

ATAACAGGGTAATTT

Light sheet time-lapse imaging of embryos

In vivo multi-position time-lapse imaging experiments (1.5 min/stack; up to 7.5 h) were conducted using a dual-illumination light sheet microscope (LS1 Live, Viventis Microscopy Sárl, Switzerland and a custom-built version of the LS1 Live microscope of identical configuration). The microscope had the following configuration: Andor Zyla 4.2 sCOMS camera; 515 nm laser to image YFP; 561 nm laser to image mCherry or mKate2; CFI75 Apochromat 25X, NA 1.1 detection objective (Nikon); scanned gaussian beam light sheet with thickness (FWHM) of 2.2 μm. The tail and PSM of growing embryos was kept in the field of view by automatically tracking the mass of the Her1-YFP signal while acquiring the timelapse and adjusting stage positions. 2 embryos were imaged in parallel in each experiment. Stacks of YFP and mCherry or mKate2 (150 planes with 1.5 μm spacing) were acquired at each position every 90 seconds.

Prior to imaging, embryos were dechorionated and placed in facility water (EPFL) with 0.02% Tricaine to prevent muscle twitching. Multiple embryos were mounted at the bottom of the light sheet microscope sample holder (Viventis Microscopy Sárl, Switzerland) and oriented laterally in agarose depressions designed to hold the yolk of an embryo and allow unhindered extension of the body and tail (Herrgen L., Schröter C., Bajard L., Oates A.C. 2009). Temperature was maintained at 28.5°C using a recirculating air heating system (Cube 2, Life Imaging Services, Swtizerland).

Image Processing of embryo timelapses

First, we defined the dataset by creating an XML file, which included all metadata and recorded transformations performed on the raw data, and saved the data in HDF5 file format (The HDF Group, 1997-2019). These two files were used in all subsequent steps. Second, to produce spatially registered timelapse movies, images were temporally registered with a linear transformation, with the first time point as a reference, using a Fiji plugin (Preibisch et al. 2014; Schindelin et al. 2012). Cellular nuclei were used as registration markers and all transformations were rigid, where the Euclidean distances between points were preserved. All of these transformations were saved in the XML file, thus the data in the HDF5 file remained unaltered. In parallel to this registration process, the notochord was segmented for each time point using a custom FIJI script. This was used as a spatial reference in the embryo, and applied to create the kymograph in Figure 2. More detail can be found at https://www.biorxiv.org/content/10.1101/2023.06.01.543221v2.

Cell Tracking in the embryo

Using Mastodon – a large-scale tracking and track-editing framework for large, multi-view images (https://github.com/mastodonsc/mastodon) – each individual cell was segmented and tracked based on nuclear signal (H2A-GFP or H2B-mCherry). We performed a semi-automatic analysis, where cells of interest were manually selected then followed by automated tracking. All tracks were manually checked and corrected. The output was the intensity for each cell, in both channels, obtained from the segmented volume (in the 3 spatial dimensions). X,Y and Z coordinates were also obtained. More detail can be found at: https://www.biorxiv.org/content/10.1101/2023.06.01.543221v2.

Data from forward tracking of PSM4 cells in a 15 somite-staged embryo (Figure 1) was only included for cells that did not divide to be comparable to our cell culture data. Backtracking of entire somites through to prospective somite S-1 (Figure 2) was done in 15-20 somite-staged embryos. Backtracking of posterior-PSM and the most recently formed somite (Figure 4) was done at 28 somite stage. Cells that were backtracked across the S-1 to S0 transition in *Tg*(*her1-YFP;mesp-ba-mKate2)* embryos (Figure 2 – figure supplement 1) were followed by first selecting rostral cells with nuclear Mesp-ba-mKate2 signal, then switching to the Her1-YFP signal tracking in the anterior PSM.

Mesp-ba-mKate2 signal-onset

To systematically define Mesp-ba-mKate2 signal-onset and its timing in the intensity traces from cells in culture and in the embryo, the steps outlined in Figure 2 – figure supplement 1 were applied.

Mesp-ba-mKate2 and Her1-YFP Somite Kymograph

Using the segmented notochord as a spatial reference in the preliminary data set, the spatial coordinates of the cells were projected to the nearest point in the notochord using Euclidean distance. This produced a new coordinate system, where cells have a reference frame in the moving and growing embryo. Each notochord segment, corresponding to the area of projected tracked cells, was then aligned over time to create a kymograph (Figure 2). Using the X and Y coordinates in the projected notochord, a matrix was built where the rows are each notochord segment over time going from posterior to anterior. The columns correspond to a binned spatial region of the

cell projection. The color code used for the Her1-YFP Kymograph was the time and position of the last peak of the cells (green). For Mesp-ba-mKate2, the signal-onset time and position (magenta) was used.

Cell Culture

Individual 15 somite-staged embryos were dechorionated in E3 then transferred into DPBS(-$CaCl_2$, -$MgCl_2$), where cells of interest were dissected out within 5 minutes. Using forceps (Dumont #5SF Forceps, straight, superfine, Fine Science Tools Item 11252-00) and a microknife (Needle Blade Microsurgical Knife Straight, Sharpoint, ref 78-6810), the skin and yolk were removed, leaving the trunk and tail intact. Holding the embryo in a lateral view, the TB was cut off posterior to the end of the notochord and the remaining AP axis up to the last formed somite boundary was quartered. PSM quarters from the desired AP level were then oriented in cross-section view so that PSM could be cut free of lateral tissue, neural tube and notochord. Dissected tissue was moved with F-127 Pluronics-coated pipette tips into coated tubes containing 50 µl DPBS(-$CaCl_2$, - $MgCl_2$). After a 5 min incubation in DPBS, the pieces were manually dissociated into single cells by brief pipetting and then transferred into wells of a 24-well glass bottom plate (Greiner Bio-One, 662896) that had been pre-coated with Protein A from Staphylococcus aureus (Sigma P6031; 100 ng/µl PA) and contained 800 µl culture media (Leibovitz's L15 Medium, no phenol red, Thermo Fisher 21083027; 50 ng/µl Protein A; 0.01% Methyl Cellulose, Sigma 274429). Surface conditions were critical to successful cultures. For example, glass surfaces should not be acid-treated, and Protein A batches and strains exhibited substantial differences. Any undissociated clusters of cells were aspirated out of the culture well using a glass needle attached to a syringe. Embryos and cells were maintained around 28.5°C throughout dissection and

dissociation. In experiments involving FGF, we added FGF8 (423-F8b R&D System) at 100ng/ml to the culture media just prior to adding the dissociated cells.

Cells were allowed to settle in the well plate on the microscope stage at 28.5°C and imaging positions were selected and focused in a 50 – 90 min window before imaging started. The time post-dissociation that imaging started was noted for each experiment in order for Her1-YFP last peak and Mesp-ba-mKate2 signal-onset timing to be compared relative to the time of dissociation rather than to the start of imaging.

To compare cells of different anteroposterior origins, PSM4 was dissected from each embryo alongside another PSM quarter of interest or TB, then cultured in an adjacent well and imaged at the same time. This provided an internal reference for arrest timing differences along the anteroposterior axis. In experiments comparing control and FGF-treated results, a starting pool of dissociated cells was split into two wells (±FGF).

Comparison of cell-autonomous Mesp-ba-mKate2 signal-onset timing in PSM4 cells from embryos that have a disabled clock (*her1-/-; her7-/-;Tg(mesp-ba-mKate2)*, with PSM4 cells from control (*Tg(mesp-ba-mKate2*) embryos was also carried out in parallel. We selected the *her1-/-; her7-/-* line because multiple studies have shown that the segmentation clock is critically crippled by the removal of two or more Hes family members from the core clock mechanism (C A Henry 2002; Lleras Forero et al. 2018; Andrew C. Oates and Ho 2002; Sari et al. 2018; Schröter et al. 2012; Zinani et al. 2021).

Our criteria for continued analysis of cells in culture was as follows: 1) alive > 5 hours post-dissociation; 2) one cell in the field of view; 3) undivided; and 4) expressed and arrested Her1-YFP.

Cell culture imaging

Cells were imaged on a Nikon Eclipse Ti (inverted) equipped with a 40x NA0.95 objective, Andor iXon897 Ultra EMCCD (512 x 512 with 16 μm pixels), Lumencor SpectraX, and hardware autofocus. Her1-YFP was detected using a Chroma 49003 filter, and Mesp-ba-mKate2 with Chroma 49008. Imaging parameters were as follows: YFP at 400 ms exposure, 4x4 binning, 1 MHz (16-bit) read-out mode, EM Gain =50, Conversion Gain=1, 510 nm LED at 20% intensity; mKate2 at 1000 ms exposure, 4x4 binning, 1 MHz (16-bit) read-out mode, EM Gain=50, Conversion Gain=1, 586 nm LED at 3% intensity; Bright field at arbitrary exposure time, no binning, 1 MHz (16-bit) read-out mode, EM Gain=50, Conversion Gain =1. Up to 120 positions with only one cell in the field of view were selected at the start of imaging per experiment. A single plane of bright field, YFP and mKate2 was captured at 10 min intervals for over 16 h using the perfect focus system. Cells remained in the center of the field of view without re-positioning throughout the movie. Temperature was controlled at 28.5 (± 0.3°C) using a stage-top incubator (Bold line, Okolab), and a light-blocking incubation chamber (Solent Scientific).

Cell culture image processing

Bright field images were passed through a custom MATLAB code for segmenting single cells. Contrast of the grayscale image of the first frame was enhanced using the adapthisteq built-in algorithm, then filtered using a guided filter (imguidedfilter, neighbourhood=3 by 3 pixels and

degree of smoothing=0.001) to preserve cell edges (regions of high variance in pixel intensity) while filtering out noise. Next, a gradient image was generated by subtracting an eroded image (imerode, disk structuring element=2 pixels) from a dilated (imdilate, disk structuring element=2 pixels) image, providing a rough outline of potential cells. Otsu's thresholding was applied to this, resulting in a binary image with several white regions (termed blobs) that represented potential cells. Given that cells were positioned approximately at the center of each image, the largest blob at the center of the image was segmented and pixel intensities in the rest of the image were set to zero (black). This served as a mask for further processing. The built-in activecontour algorithm (300 iterations, Chan-Vese method, smooth factor=1, contraction bias=0.1) was then applied on the gradient image with the mask serving as the initial state of the algorithm. The boundaries of the object region in the mask (in white) define the initial contour position used for contour evolution that ultimately segments the cell. Output from the algorithm represented the segmented cell. Fluorescent intensities from the segmented region were then determined for further analysis. Segmentation of each frame was confirmed manually and corrected when necessary.

Mesp-ba-Kate signal in her1$^{-/-}$;her7$^{-/-}$ and control PSM4 cells in culture was detected as Maximum Intensity within a manually placed ROI around the cell in Fiji.

Her1-YFP intensity trace peaks and period

Cells in culture: The high signal to noise of the intensity traces allowed the oscillatory region to be determined by visual inspection. To find the position of the peaks within this region, we used the MATLAB findpeaks function. A second order polynominal fit was performed using the intensity at the maximum, and right before/after it in order to optimise the peak positions.

Oscillatory cycles were defined between peaks. Intensity at peaks (I+) and troughs (I-) was also found.

Cells in the embryo: Peaks and troughs were defined using the entire intensity trace of Her1-YFP. The peaks and troughs of these oscillations were then calculated using the Scientific Python library's peak finder (scipy.signal.find_peaks) (SciPy 1.0 Contributors et al. 2020). A single set of parameters (width, distance and prominence) were chosen for peak identification in all intensity traces. Oscillatory cycles were calculated following the same method used for the cells in culture.

FGF-treated PSM4 and control cells in culture: Peaks and troughs were defined using the Scientific Python library's peak finder (scipy.signal.find_peaks) (SciPy 1.0 Contributors et al. 2020) and manual curation was necessary for PSM4 + FGF cells.

Acknowledgements

Our thanks to the following: F. Jülicher, A. Aulehla, M. Ebisuya, J. Garcia-Ojalvo, M. Gonzalez-Gaitan, C-P Heisenberg, A. Martinez Arias, G. Mönke, L. Morelli, C. Mulas, B. Steventon, K. Uriu, and Oates lab members for comments on the manuscript; D. Rohde for an X; J-Y Tinevez and T. Pietzsch for Mastodon assistance; MPI-CBG, UCL, and EPFL fish facilities, particularly F. Lang; U. Schulze and A. Boni for imaging help; C. Helsens for data management and C. Jollivet and V. Sergy for technical support.

Funding:

Swiss Federal Institute of Technology in Lausanne EPFL (AO)

Francis Crick Institute (AO)

Max-Planck-Gesellshaft (AO)

Wellcome Trust Senior Research Fellowship in Basic Biomedical Science WT098025MA (AO)

Long-Term HFSP postdoctoral fellowship LT000078/2016 and Whitaker International Fellowship (RAD)

Author contributions:

Conceptualization: LAR, ABR, ACO

Methodology: LAR, ABR, GV, SRN, RAD, PS, DS

Investigation: LAR, ABR, GV, SRN, RAD

Visualization: ABR, LAR, ACO

Software: ABR, SRN, PS

Funding acquisition: ACO

Supervision: ACO

Writing – Original Draft Preparation: LAR

Writing – Review & Editing: LAR, ABR, ACO

Competing Interests: PS is a co-founder of Viventis Microscopy.

Data and code availability: All movies are available upon request. All data and code from image processing through to the paper figures are provided at https://github.com/EPFL-TOP/WSC_NotebooksPaper/. Code for segmentation of bright-field images of cells can be downloaded https://github.com/sundar07/ClockTimer.

Supplementary Materials

Figure 1-4 supplement figures

References

Akiyama, R., M. Masuda, S. Tsuge, Y. Bessho, and T. Matsui. 2014. 'An Anterior Limit of FGF/Erk Signal Activity Marks the Earliest Future Somite Boundary in Zebrafish'. *Development* 141 (5): 1104–9. https://doi.org/10.1242/dev.098905.

Ambros, Victor. 2011. 'MicroRNAs and Developmental Timing'. *Current Opinion in Genetics & Development* 21 (4): 511–17. https://doi.org/10.1016/j.gde.2011.04.003.

Attardi, Andrea, Timothy Fulton, Maria Florescu, Gopi Shah, Leila Muresan, Martin O. Lenz, Courtney Lancaster, Jan Huisken, Alexander van Oudenaarden, and Benjamin Steventon. 2018. Neuromesodermal Progenitors Are a Conserved Source of Spinal Cord with Divergent Growth Dynamics (Doi: 10.1242/Dev.166728)'. *Development* 145: dev166728. https://doi.org/10.1242/dev.166728.

Aulehla, A., and O. Pourquie. 2010. 'Signaling Gradients during Paraxial Mesoderm Development'. *Cold Spring Harbor Perspectives in Biology* 2 (2): a000869–a000869. https://doi.org/10.1101/cshperspect.a000869.

Aulehla, Alexander, and Olivier Pourquié. 2006. 'On Periodicity and Directionality of Somitogenesis'. *Brain Structure and Function* 211 (S1): 3–8. https://doi.org/10.1007/s00429-006-0124-y.

Aulehla, Alexander, Christian Wehrle, Beate Brand-Saberi, Rolf Kemler, Achim Gossler, Benoit Kanzler, and Bernhard G Herrmann. 2003. 'Wnt3a Plays a Major Role in the Segmentation Clock Controlling Somitogenesis'. *Developmental Cell* 4 (3): 395–406. https://doi.org/10.1016/S1534-5807(03)00055-8.

Aulehla, Alexander, Winfried Wiegraebe, Valerie Baubet, Matthias B. Wahl, Chuxia Deng, Makoto Taketo, Mark Lewandoski, and Olivier Pourquié. 2008. 'A β-Catenin Gradient Links the Clock and Wavefront Systems in Mouse Embryo Segmentation'. *Nature Cell Biology* 10 (2): 186–93. https://doi.org/10.1038/ncb1679.

Ay, A., J. Holland, A. Sperlea, G. S. Devakanmalai, S. Knierer, S. Sangervasi, A. Stevenson, and E. M. Ozbudak. 2014. 'Spatial Gradients of Protein-Level Time Delays Set the Pace of the Traveling Segmentation Clock Waves'. *Development* 141 (21): 4158–67. https://doi.org/10.1242/dev.111930.

Boareto, Marcelo, Tomas Tomka, and Dagmar Iber. 2021. 'Positional Information Encoded in the Dynamic Differences between Neighboring Oscillators during Vertebrate Segmentation'. *Cells & Development*, September, 203737. https://doi.org/10.1016/j.cdev.2021.203737.

Brend, Tim, and Scott A. Holley. 2009. 'Expression of the Oscillating Gene *Her1* Is Directly Regulated by Hairy/Enhancer of Split, T-Box, and Suppressor of Hairless Proteins in the Zebrafish Segmentation Clock'. *Developmental Dynamics* 238 (11): 2745–59. https://doi.org/10.1002/dvdy.22100.

Brink, Susanne C. van den, Anna Alemany, Vincent van Batenburg, Naomi Moris, Marloes Blotenburg, Judith Vivié, Peter Baillie-Johnson, et al. 2020. 'Single-Cell and Spatial Transcriptomics Reveal Somitogenesis in Gastruloids'. *Nature* 582 (7812): 405–9. https://doi.org/10.1038/s41586-020-2024-3.

Brody, Thomas, and Ward F Odenwald. 2000. 'Programmed Transformations in Neuroblast Gene Expression during Drosophila CNS Lineage Development'. *Developmental Biology* 226 (1): 34–44. https://doi.org/10.1006/dbio.2000.9829.

Cooke, J, and E C Zeeman. 1976. 'A Clock and Wavefront Model for Control of the Number of Repeated Structures during Animal Morphogenesis.' *Journal of Theoretical Biology* 58 (2): 455–76.

Cutty, Stephen J., Rita Fior, Pedro M. Henriques, Leonor Saúde, and Fiona C. Wardle. 2012. 'Identification and Expression Analysis of Two Novel Members of the Mesp Family in Zebrafish'. *The International Journal of Developmental Biology* 56 (4): 285–94. https://doi.org/10.1387/ijdb.113447sc.

Danino, Tal, Octavio Mondragón-Palomino, Lev Tsimring, and Jeff Hasty. 2010. 'A Synchronized Quorum of Genetic Clocks'. *Nature* 463 (7279): 326–30. https://doi.org/10.1038/nature08753.

Delaune, Emilie A., Paul François, Nathan P. Shih, and Sharon L. Amacher. 2012. 'Single-Cell-Resolution Imaging of the Impact of Notch Signaling and Mitosis on Segmentation Clock Dynamics'. *Developmental Cell* 23 (5): 995–1005. https://doi.org/10.1016/j.devcel.2012.09.009.

Diaz Cuadros, Margarete, and Olivier Pourquie. 2021. '*In Vitro* Systems: A New Window to the Segmentation Clock'. *Development, Growth & Differentiation*, January, dgd.12710. https://doi.org/10.1111/dgd.12710.

Diaz-Cuadros, Margarete, Daniel E. Wagner, Christoph Budjan, Alexis Hubaud, Oscar A. Tarazona, Sophia Donelly, Arthur Michaut, et al. 2020. 'In Vitro Characterization of the Human Segmentation Clock'. *Nature* 580 (7801): 113–18. https://doi.org/10.1038/s41586-019-1885-9.

Diernfellner, Axel C.R., and Michael Brunner. 2020. 'Phosphorylation Timers in the Neurospora Crassa Circadian Clock'. *Journal of Molecular Biology* 432 (12): 3449–65. https://doi.org/10.1016/j.jmb.2020.04.004.

Dill, Kariena K., and Sharon L. Amacher. 2005. 'Tortuga Refines Notch Pathway Gene Expression in the Zebrafish Presomitic Mesoderm at the Post-Transcriptional Level'. *Developmental Biology* 287 (2): 225–36. https://doi.org/10.1016/j.ydbio.2005.07.032.

Dubrulle, Julien, Michael J. McGrew, and Olivier Pourquié. 2001. 'FGF Signaling Controls Somite Boundary Position and Regulates Segmentation Clock Control of Spatiotemporal Hox Gene Activation'. *Cell* 106 (2): 219–32. https://doi.org/10.1016/S0092-8674(01)00437-8.

Dubrulle, Julien, and Olivier Pourquié. 2004. 'Fgf8 mRNA Decay Establishes a Gradient That Couples Axial Elongation to Patterning in the Vertebrate Embryo.' *Nature* 427 (6973): 419–22. https://doi.org/10.1038/nature02216.

Elmasri, Harun, Christoph Winkler, Daniel Liedtke, Takao Sasado, Chikako Morinaga, Hiroshi Suwa, Katsutoshi Niwa, et al. 2004. 'Mutations Affecting Somite Formation in the Medaka (Oryzias Latipes)'. *Mechanisms of Development* 121 (7–8): 659–71. https://doi.org/10.1016/j.mod.2004.04.003.

Henry, C A. 2002. 'Two Linked Hairy/Enhancer of Split-Related Zebrafish Genes, Her1 and Her7, Function Together to Refine Alternating Somite Boundaries', no. 129, 12.

Henry, Clarissa A., Cara T. Poage, Matthew B. McCarthy, Jose Campos-Ortega, and Mark S. Cooper. 2005. 'Regionally Autonomous Segmentation Within Zebrafish Presomitic Mesoderm'. *Zebrafish* 2 (1): 7–18. https://doi.org/10.1089/zeb.2005.2.7.

Herrgen L., Schröter C., Bajard L., Oates A.C. 2009. 'Multiple Embryo Time-Lapse Imaging of Zebrafish Development.' In *Zebrafish. Methods in Molecular Biology (Methods and Protocols)*. Vol. 546. Humana Press.

Hubaud, Alexis, and Olivier Pourquié. 2014. 'Signalling Dynamics in Vertebrate Segmentation'. *Nature Reviews Molecular Cell Biology* 15 (11): 709–21. https://doi.org/10.1038/nrm3891.

Hubaud, Alexis, Ido Regev, L. Mahadevan, and Olivier Pourquié. 2017. 'Excitable Dynamics and Yap-Dependent Mechanical Cues Drive the Segmentation Clock'. *Cell*, September. https://doi.org/10.1016/j.cell.2017.08.043.

Langenberg, Tobias, Michael Brand, and Mark S. Cooper. 2003. 'Imaging Brain Development and Organogenesis in Zebrafish Using Immobilized Embryonic Explants'. *Developmental Dynamics* 228 (3): 464–74. https://doi.org/10.1002/dvdy.10395.

Lauschke, Volker M., Charisios D. Tsiairis, Paul François, and Alexander Aulehla. 2013. 'Scaling of Embryonic Patterning Based on Phase-Gradient Encoding'. *Nature* 493 (7430): 101–5. https://doi.org/10.1038/nature11804.

Lleras Forero, Laura, Rachna Narayanan, Leonie FA Huitema, Maaike VanBergen, Alexander Apschner, Josi Peterson-Maduro, Ive Logister, et al. 2018. 'Segmentation of the Zebrafish Axial Skeleton Relies on Notochord Sheath Cells and Not on the Segmentation Clock'. *eLife* 7 (April):e33843. https://doi.org/10.7554/eLife.33843.

Mara, Andrew, Joshua Schroeder, Cécile Chalouni, and Scott A. Holley. 2007. 'Priming, Initiation and Synchronization of the Segmentation Clock by deltaD and deltaC'. *Nature Cell Biology* 9 (5): 523–30. https://doi.org/10.1038/ncb1578.

Maroto, Miguel, J. Kim Dale, Mary-Lee Dequeant, Anne-Cecile Petit, and Olivier Pourquie. 2005. 'Synchronised Cycling Gene Oscillations in Presomitic Mesoderm Cells Require Cell-Cell Contact'. *The International Journal of Developmental Biology* 49 (2–3): 309–15. https://doi.org/10.1387/ijdb.041958mm.

Martin, Benjamin L. 2016. 'Factors That Coordinate Mesoderm Specification from Neuromesodermal Progenitors with Segmentation during Vertebrate Axial Extension'. *Seminars in Cell & Developmental Biology*, Bone development and diseaseMechanisms of vertebrate embryo segmentation, 49 (January):59–67. https://doi.org/10.1016/j.semcdb.2015.11.014.

Masamizu, Yoshito, Toshiyuki Ohtsuka, Yoshiki Takashima, Hiroki Nagahara, Yoshiko Takenaka, Kenichi Yoshikawa, Hitoshi Okamura, and Ryoichiro Kageyama. 2006. 'Real-Time Imaging of the Somite Segmentation Clock: Revelation of Unstable Oscillators in the Individual Presomitic Mesoderm Cells'. *Proceedings of the National Academy of Sciences* 103 (5): 1313–18. http://www.pnas.org/content/103/5/1313.short.

Matsuda, Mitsuhiro, Hanako Hayashi, Jordi Garcia-Ojalvo, Kumiko Yoshioka-Kobayashi, Ryoichiro Kageyama, Yoshihiro Yamanaka, Makoto Ikeya, Junya Toguchida, Cantas Alev, and Miki Ebisuya. 2020. 'Species-Specific Segmentation Clock Periods Are Due to Differential Biochemical Reaction Speeds'. *Science* 369 (6510): 1450–55. https://doi.org/10.1126/science.aba7668.

Matsuda, Mitsuhiro, Yoshihiro Yamanaka, Maya Uemura, Mitsujiro Osawa, Megumu K. Saito, Ayako Nagahashi, Megumi Nishio, et al. 2020. 'Recapitulating the Human Segmentation Clock with Pluripotent Stem Cells'. *Nature* 580 (7801): 124–29. https://doi.org/10.1038/s41586-020-2144-9.

Matsumiya, Marina, Takehito Tomita, Kumiko Yoshioka-Kobayashi, Akihiro Isomura, and Ryoichiro Kageyama. 2018. 'ES Cell-Derived Presomitic Mesoderm-like Tissues for Analysis of Synchronized Oscillations in the Segmentation Clock'. *Development* 145 (4): dev156836. https://doi.org/10.1242/dev.156836.

Morelli, Luis G., Saúl Ares, Leah Herrgen, Christian Schröter, Frank Jülicher, and Andrew C. Oates. 2009. 'Delayed Coupling Theory of Vertebrate Segmentation'. *HFSP Journal* 3 (1): 55–66. https://doi.org/10.2976/1.3027088.

Moreno, Tanya a., and Chris Kintner. 2004. 'Regulation of Segmental Patterning by Retinoic Acid Signaling during Xenopus Somitogenesis'. *Developmental Cell* 6:205–18. https://doi.org/10.1016/S1534-5807(04)00026-7.

Murray, Philip J., Philip K. Maini, and Ruth E. Baker. 2011. 'The Clock and Wavefront Model Revisited'. *Journal of Theoretical Biology* 283 (1): 227–38. https://doi.org/10.1016/j.jtbi.2011.05.004.

Negrete JR, Jose, Ivan M Lengyel, Laurel A Rohde, Ravi A Desai, Andrew Oates, and Frank Jülicher. 2021. 'Theory of Time Delayed Genetic Oscillations with External Noisy Regulation'. *New Journal of Physics*, January. https://doi.org/10.1088/1367-2630/abd80b.

Oates, A. C., L. G. Morelli, and S. Ares. 2012. 'Patterning Embryos with Oscillations: Structure, Function and Dynamics of the Vertebrate Segmentation Clock'. *Development* 139 (4): 625–39. https://doi.org/10.1242/dev.063735.

Oates, Andrew C. 2020. 'Waiting on the Fringe: Cell Autonomy and Signaling Delays in Segmentation Clocks'. *Current Opinion in Genetics & Development* 63 (August):61–70. https://doi.org/10.1016/j.gde.2020.04.008.

Oates, Andrew C., and Robert K. Ho. 2002. 'Hairy/E (Spl)-Related (Her) Genes Are Central Components of the Segmentation Oscillator and Display Redundancy with the Delta/Notch Signaling Pathway in the Formation of Anterior Segmental Boundaries in the Zebrafish'. *Development* 129 (12): 2929–46. http://dev.biologists.org/content/129/12/2929.short.

Palmeirim, I, D Henrique, D Ish-Horowicz, and O Pourquié. 1997. 'Avian Hairy Gene Expression Identifies a Molecular Clock Linked to Vertebrate Segmentation and Somitogenesis.' *Cell* 91 (5): 639–48. https://doi.org/10.1016/S0092-8674(00)80451-1.

Palmeirim, Isabel, Julien Dubrulle, Domingos Henrique, David Ish-Horowicz, and Olivier Pourquié. 1998. 'Uncoupling Segmentation and Somitogenesis in the Chick Presomitic Mesoderm'. *Developmental Genetics* 23:77–85. https://doi.org/10.1002/(SICI)1520-6408(1998)23:1<77::AID-DVG8>3.0.CO;2-3.

Pourquié, Olivier. 2022. 'A Brief History of the Segmentation Clock'. *Developmental Biology* 485 (May):24–36. https://doi.org/10.1016/j.ydbio.2022.02.011.

Preibisch, Stephan, Fernando Amat, Evangelia Stamataki, Mihail Sarov, Robert H Singer, Eugene Myers, and Pavel Tomancak. 2014. 'Efficient Bayesian-Based Multiview Deconvolution'. *Nature Methods* 11 (6): 645–48. https://doi.org/10.1038/nmeth.2929.

Recher, G., J. Jouralet, A. Brombin, A. Heuze, E. Mugniery, J.-M. Hermel, S. Desnoulez, et al. 2013. 'Zebrafish Midbrain Slow-Amplifying Progenitors Exhibit High Levels of Transcripts for Nucleotide and Ribosome Biogenesis'. *Development* 140 (24): 4860–69. https://doi.org/10.1242/dev.099010.

Sanaki-Matsumiya, Marina, Mitsuhiro Matsuda, Nicola Gritti, Fumio Nakaki, James Sharpe, Vikas Trivedi, and Miki Ebisuya. 2022. 'Periodic Formation of Epithelial Somites from Human Pluripotent Stem Cells'. *Nature Communications* 13 (1): 2325. https://doi.org/10.1038/s41467-022-29967-1.

Sari, Dini Wahyu Kartika, Ryutaro Akiyama, Honda Naoki, Hannosuke Ishijima, Yasumasa Bessho, and Takaaki Matsui. 2018. 'Time-Lapse Observation of Stepwise Regression of

Erk Activity in Zebrafish Presomitic Mesoderm'. *Scientific Reports* 8 (1). https://doi.org/10.1038/s41598-018-22619-9.

Sawada, Atsushi, Minori Shinya, Yun-Jin Jiang, Atsushi Kawakami, Atsushi Kuroiwa, and Hiroyuki Takeda. 2001. 'Fgf/MAPK Signalling Is a Crucial Positional Cue in Somite Boundary Formation'. *Development* 128 (23): 4873–80. http://dev.biologists.org/content/128/23/4873.short.

Schindelin, Johannes, Ignacio Arganda-Carreras, Erwin Frise, Verena Kaynig, Mark Longair, Tobias Pietzsch, Stephan Preibisch, et al. 2012. 'Fiji: An Open-Source Platform for Biological-Image Analysis'. *Nature Methods* 9 (7): 676–82. https://doi.org/10.1038/nmeth.2019.

Schröter, Christian, Saúl Ares, Luis G. Morelli, Alina Isakova, Korneel Hens, Daniele Soroldoni, Martin Gajewski, et al. 2012. 'Topology and Dynamics of the Zebrafish Segmentation Clock Core Circuit'. Edited by Kate G. Storey. *PLoS Biology* 10 (7): e1001364. https://doi.org/10.1371/journal.pbio.1001364.

SciPy 1.0 Contributors, Pauli Virtanen, Ralf Gommers, Travis E. Oliphant, Matt Haberland, Tyler Reddy, David Cournapeau, et al. 2020. 'SciPy 1.0: Fundamental Algorithms for Scientific Computing in Python'. *Nature Methods* 17 (3): 261–72. https://doi.org/10.1038/s41592-019-0686-2.

Shih, N. P., P. Francois, E. A. Delaune, and S. L. Amacher. 2015. 'Dynamics of the Slowing Segmentation Clock Reveal Alternating Two-Segment Periodicity'. *Development* 142 (10): 1785–93. https://doi.org/10.1242/dev.119057.

Simsek, M. Fethullah, and Ertuğrul M. Özbudak. 2018. 'Spatial Fold Change of FGF Signaling Encodes Positional Information for Segmental Determination in Zebrafish'. *Cell Reports* 24 (1): 66-78.e8. https://doi.org/10.1016/j.celrep.2018.06.023.

Sonnen, Katharina F., Volker M. Lauschke, Julia Uraji, Henning J. Falk, Yvonne Petersen, Maja C. Funk, Mathias Beaupeux, Paul François, Christoph A. Merten, and Alexander Aulehla. 2018. 'Modulation of Phase Shift between Wnt and Notch Signaling Oscillations Controls Mesoderm Segmentation'. *Cell* 172 (5): 1079-1090.e12. https://doi.org/10.1016/j.cell.2018.01.026.

Soroldoni, D., D. J. Jorg, L. G. Morelli, D. L. Richmond, J. Schindelin, F. Julicher, and A. C. Oates. 2014. 'A Doppler Effect in Embryonic Pattern Formation'. *Science* 345 (6193): 222–25. https://doi.org/10.1126/science.1253089.

Tsiairis, Charisios D., and Alexander Aulehla. 2016. 'Self-Organization of Embryonic Genetic Oscillators into Spatiotemporal Wave Patterns'. *Cell* 164 (4): 656–67. https://doi.org/10.1016/j.cell.2016.01.028.

Venzin, Olivier F., and Andrew C. Oates. 2020. 'What Are You Synching about? Emerging Complexity of Notch Signaling in the Segmentation Clock'. *Developmental Biology* 460 (1): 40–54. https://doi.org/10.1016/j.ydbio.2019.06.024.

Wanglar, Chimwar, Jun Takahashi, Taijiro Yabe, and Shinji Takada. 2014. 'Tbx Protein Level Critical for Clock-Mediated Somite Positioning Is Regulated through Interaction between Tbx and Ripply'. Edited by Moises Mallo. *PLoS ONE* 9 (9): e107928. https://doi.org/10.1371/journal.pone.0107928.

Webb, Alexis B, Iván M Lengyel, David J Jörg, Guillaume Valentin, Frank Jülicher, Luis G Morelli, and Andrew C Oates. 2016. 'Persistence, Period and Precision of Autonomous Cellular Oscillators from the Zebrafish Segmentation Clock'. *eLife* 5 (February):e08438. https://doi.org/10.7554/eLife.08438.

Yabe, Taijiro, Koichiro Uriu, and Shinji Takada. 2023. 'Ripply Suppresses Tbx6 to Induce Dynamic-to-Static Conversion in Somite Segmentation'. *Nature Communications* 14 (1): 2115. https://doi.org/10.1038/s41467-023-37745-w.

Yoshioka-Kobayashi, Kumiko, Marina Matsumiya, Yusuke Niino, Akihiro Isomura, Hiroshi Kori, Atsushi Miyawaki, and Ryoichiro Kageyama. 2020. 'Coupling Delay Controls Synchronized Oscillation in the Segmentation Clock'. *Nature* 580 (7801): 119–23. https://doi.org/10.1038/s41586-019-1882-z.

Zákány, József, Marie Kmita, Pilar Alarcon, José-Luis de la Pompa, and Denis Duboule. 2001. 'Localized and Transient Transcription of Hox Genes Suggests a Link between Patterning and the Segmentation Clock'. *Cell* 106 (2): 207–17. https://doi.org/10.1016/S0092-8674(01)00436-6.

Zinani, Oriana Q. H., Kemal Keseroğlu, Ahmet Ay, and Ertuğrul M. Özbudak. 2021. 'Pairing of Segmentation Clock Genes Drives Robust Pattern Formation'. *Nature* 589 (7842): 431–36. https://doi.org/10.1038/s41586-020-03055-0.